Systematic study of microscopic nuclear level densities of Sn isotopes within a relativistic framework*

Guanbin He (何冠彬)[1] Nuocheng Tang (唐诺程)[1] Yuan Tian (田源)[1†] Ying Cui (崔莹)[1]
Jian Li (李剑)[2] Yi Xu (徐毅)[1,3‡] Ruirui Xu (续瑞瑞)[1§]

[1]China Nuclear Data Center, China Institute of Atomic Energy, Beijing 102413, China
[2]College of Physics, Jilin University, Changchun 130012, China
[3]Extreme Light Infrastructure - Nuclear Physics (ELI-NP), Horia Hulubei National Institute for R&D in Physics and Nuclear Engineering (IFIN-HH), 077125 Bucharest-Magurele, Romania

Abstract: Nuclear level density (NLD) plays a crucial role in describing the statistical properties of excited nuclei and is a key input for models of compound nuclear reactions, such as those used in nuclear astrophysics and reactor physics. In this study, we construct microscopic nuclear level densities for Sn isotopes by combining single-particle spectra, pairing correlations, and deformation parameters derived from relativistic Hartree–Bogoliubov (RHB) calculations with the combinatorial method. We examine the energy dependence and isotopic systematics of the calculated level densities. In particular, we analyze their variation with excitation energy and neutron number, and compare them to available experimental data, including cumulative low-lying levels and *s*-wave neutron resonance spacings (D_0). The resulting level densities are further employed as input to Hauser–Feshbach calculations of radiative neutron capture (n,γ) cross-sections [Nuclear Data Sheets **120**, 272 (2014)]. Our results demonstrate that RHB-based nuclear level densities provide a reliable microscopic framework for describing Sn isotopic level densities and accurately predicting (n,γ) cross-sections.

Keywords: microscopic nuclear level densities, Relativistic Hartree–Bogoliubov theory, combinatorial method, nuclear reaction calculation

DOI: 10.1088/1674-1137/ae4329 **CSTR:** 32044.14.ChinesePhysicsC.50054107

I. INTRODUCTION

Nuclear level density (NLD), which characterizes the number of excited states per unit energy in an atomic nucleus, is a fundamental quantity in nuclear structure and reaction theory. It is a key input for the calculation of reaction cross-sections relevant to nucleosynthesis and other applications [1−6]. Within statistical reaction models, the NLD governs decay widths and determines the competition among different reaction channels.

Traditionally, nuclear level densities have been described using phenomenological models, such as the constant temperature model (CTM) [7], back-shifted Fermi gas model (BSM) [8], and generalized superfluid model (GSM) [9]. While computationally efficient, these models rely on parameters adjusted to experimental data and therefore lack a firm microscopic foundation. Moreover, experimental information on nuclear level densities remains limited, especially for nuclei positioned far from the β-stability line [10], and this limitation restricts the predictive power of purely phenomenological approaches.

Over the past decades, a variety of microscopic approaches to determine NLDs have been developed. These include the equidistant spacing model [11−14], the shell-model-based Monte Carlo method [15−19], spectral distribution calculations [20−22], finite-temperature independent-particle models [23−26], microstatistical approaches [27−30], and random matrix theories [31]. Among these methods, microscopic level densities based on the nonrelativistic Hartree–Fock–Bogoliubov (HFB) theory, combined with the combinatorial method, have been widely applied and shown to provide a quantitative description of experimental data [28, 32−36].

Received 16 January 2026; Accepted 9 February 2026; Accepted manuscript online 10 February 2026

* Supported by the National Key Research and Development (R&D) Program (2022YFA1602403), the "Ye Qisun" Science Foundation of the National Natural Science Foundation of China (U2541242), the Key Program of the National Natural Science Foundation of China (KZ77088701), the National Natural Science Foundation of China (U2441221), and the IAEA Research Contract (28681)

† E-mail: tiany@ciae.ac.cn
‡ E-mail: yi.xu@eli-np.ro
§ E-mail: xuruirui@ciae.ac.cn

Notably, microscopic nuclear level densities are not restricted to nonrelativistic frameworks. In recent years, relativistic approaches based on the relativistic Hartree–Bogoliubov (RHB) theory have also been applied to the study of nuclear level densities. In particular, calculations employing the covariant density functional theory have been reported for selected nuclei, demonstrating the feasibility of constructing microscopic level densities within a relativistic framework [37, 38].

Nevertheless, compared to nonrelativistic HFB-based approaches, systematic investigations of microscopic level densities within a relativistic framework remain limited, particularly along extended isotopic chains. Moreover, validations of relativistic microscopic level densities through reaction observables, such as radiative neutron capture cross-sections, have been rarely reported. Therefore, further studies are required to assess the predictive power and practical applicability of relativistic level-density models.

The Sn isotopic chain ($Z = 50$) provides an ideal testing ground for microscopic NLD studies. The proton shell closure at $Z = 50$ simplifies the underlying structural evolution, and the isotopic sequence from ^{100}Sn to ^{132}Sn spans a wide range of neutron numbers, including the $N = 50$ and $N = 82$ shell closures. Additionally, a wealth of experimental information is available for Sn isotopes, such as *s*-wave neutron resonance spacings (D_0) [9], cumulative numbers of low-lying discrete levels [39], and radiative neutron capture (n,γ) cross-sections [40], allowing for a comprehensive validation of theoretical calculations.

Building on the aforementioned considerations, in this study, we systematically investigate the microscopic NLDs along the Sn isotopic chain. Using single-particle energies, pairing gaps, and deformation parameters obtained from RHB calculations [41, 42], microscopic level densities are constructed for Sn isotopes from ^{111}Sn to ^{124}Sn. This approach allows for a detailed analysis of their energy dependence, isotopic trends, and performance in nuclear reaction calculations. These reliable microscopic level densities are crucial for nuclear structure studies as well as for nuclear reaction modeling and data evaluation, especially for neutron-induced reactions in nuclear technology and astrophysical applications.

II. THEORETICAL FRAMEWORK

In this study, microscopic NLDs are constructed by combining self-consistent RHB calculations with the combinatorial method. The RHB framework provides single-particle energies, pairing gaps, and deformation properties, which constitute the microscopic input for the enumeration of particle–hole excitation configurations. On this basis, the combinatorial method enables a direct microscopic evaluation of NLDs as functions of excitation energies.

A. RHB theory

CDFT provides a relativistic framework for the self-consistent description of nuclear mean-field properties. Within this framework, the RHB theory treats particle–hole and particle–particle correlations on an equal footing through the Bogoliubov transformation.

In the RHB framework, the quasiparticle wave functions U_k and V_k are obtained by solving the RHB equations [42]:

$$\begin{pmatrix} \hat{h}_D - \lambda & \hat{\Delta} \\ -\hat{\Delta}^* & -\hat{h}_D + \lambda \end{pmatrix} \begin{pmatrix} U_k \\ V_k \end{pmatrix} = E_k \begin{pmatrix} U_k \\ V_k \end{pmatrix}, \quad (1)$$

where $\hat{h}_D$ denotes the Dirac Hamiltonian, λ is the Fermi energy, $\hat{\Delta}$ is the pairing field, and E_k is the quasiparticle energy.

The Dirac Hamiltonian is given by

$$\hat{h}_D = \boldsymbol{\alpha} \cdot \boldsymbol{p} + V + \beta(M + S), \quad (2)$$

where $\boldsymbol{\alpha}$ and β are Dirac matrices, M denotes the nucleon mass, and S and V are the scalar and vector mean fields potential, respectively. In the present calculations, the density-dependent meson–nucleon coupling functional DD-ME2 is adopted [43].

The pairing field $\hat{\Delta}$ is defined as

$$\hat{\Delta} = \frac{1}{2} \sum_{n_1 n_2} V^{pp}_{n_1 n_2} \kappa_{n_1 n_2}, \quad (3)$$

where V^{pp} denotes the pairing interaction, and κ is the pairing tensor (the sum runs over single-particle states). In the present calculations, a separable pairing interaction is employed [44, 45], which allows for an efficient treatment of pairing correlations in coordinate space. The corresponding pairing interaction can be expressed as

$$V(\boldsymbol{r}_1, \boldsymbol{r}_2, \boldsymbol{r}'_1, \boldsymbol{r}'_2) = -G\,\delta(\boldsymbol{R} - \boldsymbol{R}')P(r)\,P(r')\frac{1}{2}(1 - P^{\sigma}), \quad (4)$$

where P^{σ} is the spin-exchange operator, and $\boldsymbol{R} = (\boldsymbol{r}_1 + \boldsymbol{r}_2)/2$ and $\boldsymbol{r} = \boldsymbol{r}_1 - \boldsymbol{r}_2$ denote the center-of-mass and relative coordinates, respectively. A Gaussian form factor $P(r)$ is adopted:

$$P(r) = \frac{1}{(4\pi a^2)^{3/2}} \exp\left(-\frac{r^2}{4a^2}\right). \quad (5)$$

The pairing-strength parameter and range are set as $G = 728$ MeV fm^3 and $a = 0.644$ fm, respectively, follow-

ing the values provided in Refs. [44, 45].

B. Combinatorial method

The combinatorial method provides a microscopic approach for the direct calculation of NLDs. In this approach, excited states are described as many-body configurations constructed from particle–hole excitations built on single-particle energy levels. By explicitly enumerating all configurations that satisfy conservation laws of excitation energy, angular momentum, and parity, nuclear level densities are obtained through direct counting of microscopic states. In contrast to analytical models based on continuous approximations, the discrete nature of the single-particle spectrum, shell effects, and quantum-number constraints is preserved.

Although pairing gaps and deformation parameters do not appear explicitly in the combinatorial counting formulas, they enter implicitly through the self-consistent quasiparticle spectrum obtained from the RHB calculations. Pairing correlations determine the quasiparticle energies via the Bogoliubov transformation, which set the excitation energies of the particle–hole configurations enumerated in the combinatorial method. Nuclear deformation affects the underlying single-particle level structure, and for axially symmetric nuclei, enters through the rotational energy correction $E_{\rm rot}^{J,K}$.

In this approach, the combinatorial formalism provides a transparent microscopic connection between the single-particle structure and the resulting NLD through an explicit configuration counting scheme.

The generating function $\mathcal{Z}$ is defined as [10]

$$\mathcal{Z}(x_1,x_2,x_3,x_4,y,t)=\prod_{k=1}^{4}\prod_{i=1}^{I_k}\left(1+x_k p_i^k y^{\varepsilon_i^k} t^{m_i^k}\right), \tag{6}$$

where y and t are the generating variables associated with the excitation energy and angular-momentum projection, respectively; x_k facilitates the counting of the number of particles and holes; ε_i^k, m_i^k and p_i^k denote the single-particle excitation energy, spin projection, and parity of the corresponding state, respectively. Expanding $\mathcal{Z}$ in powers of x_k yields

$$\mathcal{Z}(x_1,x_2,x_3,x_4,y,t)=\sum_{\mathcal{N}}\mathcal{F}_{\mathcal{N}}(y,t)\prod_{k=1}^{4}x_k^{N_k}, \tag{7}$$

where $\mathcal{N}=(N_1,N_2,N_3,N_4)$ specifies the numbers of proton holes, proton particles, neutron holes, and neutron particles. Further expansion of $\mathcal{F}_{\mathcal{N}}(y,t)$ in powers of y and t gives

$$\mathcal{F}_{\mathcal{N}}(y,t)=\sum_{U}\sum_{M}\sum_{P=\pm1}C_{\mathcal{N}}(U,M,P)\,y^U t^M, \tag{8}$$

where $C_{\mathcal{N}}(U,M,P)$ denotes the number of particle–hole configurations with excitation energy U, spin projection M, and parity P.

The intrinsic state density ρ_i at a given excitation energy is defined as

$$\rho_i(U,M,P)=\frac{C(U,M,P)}{\varepsilon_0}, \tag{9}$$

where $C(U,M,P)$ is the number of the folded states in the unit energy ε_0.

The intrinsic state density accounts for only incoherent particle–hole excitations. Collective effects, in particular rotational and vibrational contributions, are included to obtain the NLD. In the present calculations, vibrational effects are treated following the approach repoprted in Ref. [46]. In this approach, low-energy phonon excitations are incorporated through a Boson partition function, and $\rho_{i*\nu}$ is determined by considering the vibrational effects.

Then, we include the rotational effects. For spherical nuclei, the intrinsic and laboratory frames coincide, and the level density is given by [1]

$$\rho(U,J,P)=\rho_{i*\nu}(U,M=J,P)-\rho_{i*\nu}(U,M=J+1,P). \tag{10}$$

For deformed nuclei with axial symmetry, rotational effects are included according to [10]

$$\begin{aligned}\rho(U,J,P)=\frac{1}{2}\sum_{K=-J,K\neq0}^{J}&\rho_{i*\nu}(U-E_{\rm rot}^{J,K},K,P)\\&+\delta_{(J\,\rm even)}\delta_{(P=+)}\rho_{i*\nu}(U-E_{\rm rot}^{J,0},0,P)\\&+\delta_{(J\,\rm odd)}\delta_{(P=-)}\rho_{i*\nu}(U-E_{\rm rot}^{J,0},0,P).\end{aligned} \tag{11}$$

where $E_{\rm rot}^{J,K}$ is the rotational energy [32, 47], K is spin projection, and P is parity.

III. RESULTS AND DISCUSSION

This section presents the results of microscopic NLDs obtained for the Sn isotopic chain. Ground-state properties obtained from RHB calculations are first discussed, followed by an analysis of the calculated level densities and their isotopic systematics. The results are compared with available experimental constraints, including *s*-wave neutron resonance spacings, and the performance of the present level densities is further examined through radiative neutron capture (n,γ) cross-section calculations.

A. Ground-state properties

The binding energies obtained from the RHB calculations are compared with experimental values in Table 1

Table 1. Theoretical and experimental binding energies, their differences, and blocking levels for odd-A nuclei (A = 111–125).

Nucleus A	RHB/MeV	Exp/MeV	ΔE/MeV	Blocking
111	940.79	942.7	+1.91	$5/2^+$
112	951.40	953.6	+2.20	–
113	959.56	961.3	+1.74	$5/2^+$
114	969.80	971.6	+1.80	–
115	977.50	979.1	+1.60	$1/2^+$
116	987.17	988.7	+1.53	–
117	994.41	995.7	+1.29	$3/2^+$
118	1003.66	1005.0	+1.34	–
119	1010.41	1011.4	+0.99	$3/2^+$
120	1019.41	1020.5	+1.09	–
121	1025.80	1026.7	+0.90	$11/2^-$
122	1034.52	1035.5	+0.98	–
123	1040.40	1041.4	+1.00	$1/2^+$
124	1049.10	1049.9	+0.80	–
125	1054.59	1055.8	+1.21	$1/2^+$

for Sn isotopes with mass numbers A = 111–125. The RHB results reproduce the overall isotopic trend of the experimental binding energies along the chain [48, 49]. A systematic underbinding is observed, with deviations ranging from approximately 0.8 to 2.2 MeV. Such deviations are typical for global covariant energy density functionals and gradually reduce as we move toward heavier isotopes, indicating improved agreement as the N = 82 shell closure is approached.

The RHB calculations predict that the Sn isotopes considered in this study are spherical or only extremely weakly deformed. Consequently, deformation effects mainly enter implicitly through the single-particle spectrum, and rotational collective enhancements are expected to be negligible.

For odd-A nuclei, blocking calculations are performed by fixing the occupation of the lowest-energy quasiparticle state with appropriate quantum numbers, as listed in Table 1. This procedure allows even–even and odd-mass nuclei to be treated on the same footing within the RHB framework, which is essential for systematic studies along isotopic chains.

In addition to binding energies, pairing correlations are quantified through the neutron three-point odd–even mass difference [50]:

$$\Delta_n^{(3)}(N) = \frac{1}{2}\left[B(N-1) - 2B(N) + B(N+1)\right], \qquad (12)$$

where $B(N)$ denotes the binding energy of the nucleus with neutron number N.

The calculated values of $\Delta_n^{(3)}(N)$ for Sn isotopes, ranging from ^{111}Sn to ^{124}Sn, are presented and compared with experimental data in Fig. 1. The RHB calculations reproduce the characteristic odd–even staggering pattern along the isotopic chain, with pairing gaps of the correct order of magnitude. The remaining deviations, typically within a few hundred keV, reflect the sensitivity of the three-point indicator to local shell effects and single-particle level spacing near the Fermi surface.

Overall, the RHB framework provides a consistent microscopic description of ground-state properties for both even–even and odd-A Sn isotopes, supplying reliable single-particle spectra and pairing correlations for the combinatorial construction of NLDs discussed below.

B. Total level density

The total nuclear level densities, $\rho(U)$, as functions of excitation energy, U, are calculated for Sn isotopes from ^{111}Sn to ^{124}Sn. To highlight the global energy dependence, Gaussian smoothing with a width of σ = 2.0 MeV is applied, as shown in Fig. 2.

For all the isotopes, the level density increases rapidly with excitation energy; however, below $U \approx 1$ MeV, the behavior is influenced by the discrete nature of the low-lying states and by pairing gaps. An approximately exponential increase becomes evident at low-to-intermediate excitation energies (~ 1–3 MeV). At higher excitation energies, the level density curves display similar slopes, indicating a gradual transition toward a regime dominated by statistical properties.

In Fig. 2, the dashed and solid curves correspond to odd-A and even–even nuclei, respectively and clearly show the odd–even staggering. Additionally, an isotopic dependence is observed. Toward the N = 82 shell closure, the level density tends to reduce, and this reduction is the most evident in the vicinity of the neutron separation en-

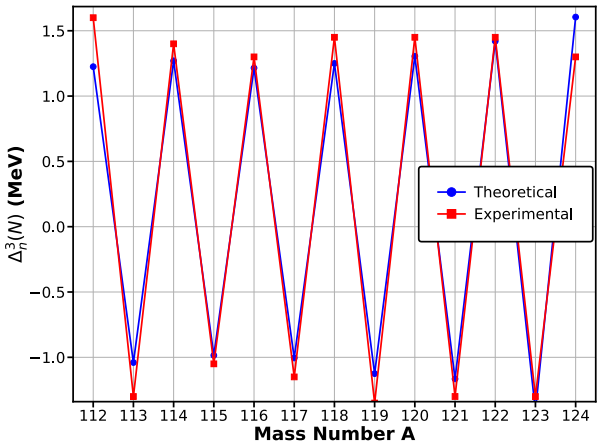

Fig. 1. (color online) Odd–even mass differences for Sn isotopes from, ^{111}Sn to ^{124}Sn, compared with experimental data.

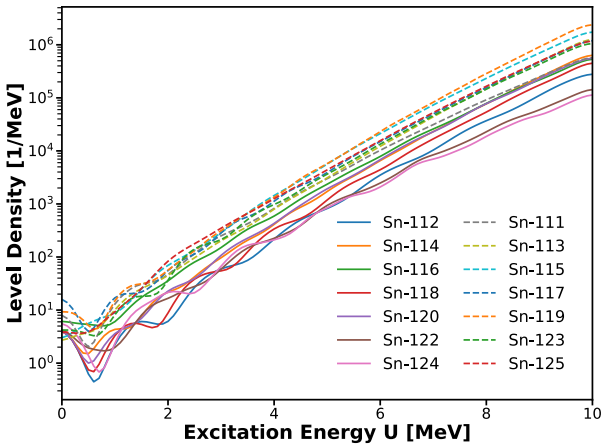

Fig. 2. (color online) Calculated level densities as a function of excitation energy for the Sn isotopic chain from ^{111}Sn to ^{124}Sn using the RHB theory combined with the combinatorial method. Odd-A nuclei are shown with dashed curves, and even–even nuclei are shown with solid curves.

ergy; this observation does not necessarily imply a strictly monotonic ordering over the full excitation-energy range.

Overall, the calculated total level densities show smooth energy dependence and consistent isotopic trends, forming the basis for comparisons with experimental constraints and reaction calculations discussed here. These systematic features of the total level densities are expected to directly influence statistical model calculations based on the compound-nucleus mechanism.

C. Comparison with experimental data and HFB-based results

The nuclear level densities of Sn isotopes, calculated using the present RHB-based approach, are compared with experimental data obtained using the Oslo method [39] as well as with results using the nonrelativistic HFB approach [51] combined with the combinatorial method. In Fig. 3, the red curves represent the current calculations; the blue dashed curves show the HFB-based results; and the red symbols indicate the experimental data.

For most isotopes, the present calculations reproduce the experimental level densities over a broad excitation-energy range. In particular, at low excitation energies, typically below 6 MeV, the RHB-based results follow both the slope and absolute magnitude of the experimental data more closely than the HFB-based calculations. By contrast, the integrated HFB–combinatorial approach tends to overestimate the level density in this energy region for several isotopes. In our calculations, the RHB theory is implemented with a finite-range separable pairing force [44, 45]. The improved agreement with experimental level densities at low excitation energies is attributed to the combined effects of pairing correlations and differences in the underlying single-particle shell structure predicted by the relativistic framework, rather than to pairing correlations alone. In particular, for mid-shell Sn isotopes such as $^{112-118}$Sn, the results obtained using the present approach show better agreement with the experimental level densities in the low-energy region, where the pairing and shell effects are the most pronounced. A detailed sensitivity study with respect to the pairing interaction is beyond the scope of this study; however, moderate variations in the pairing strength are expected to mainly affect low-energy level densities, and the overall isotopic trends are expected to remain robust.

At excitation energies approximately equal to the neutron separation energy S_n, the present level densities are constrained by the available experimental information on s-wave neutron resonance spacings. A quantitative comparison is presented in Table 2, which lists the calculated and experimental D_0 values for selected Sn isotopes [9]. The s-wave neutron resonance spacing (D_0) is determined from the level density at the neutron separation energy, $\rho(S_n)$, combined with the corresponding spin–parity distributions, following standard nuclear data evaluation methods.

The present calculations reproduce the overall isotopic trend of the experimental D_0 values. The calculated spacings are typically within a factor of 2–3 of the experimental data; this factor is comparable to the accuracy commonly achieved by microscopic level-density models. This excellent agreement between the results indicates that the present microscopic level densities are suitable for use in statistical reaction calculations and nuclear data applications.

D. Radiative neutron capture (n,γ) cross-sections

Radiative neutron capture (n,γ) cross-sections are calculated within the statistical Hauser–Feshbach framework using the UNF code [52−54]. The UNF framework integrates the optical model, the Hauser–Feshbach model, and an exciton model, which incorporates angular-momentum-dependent effects, thus improving the treatment of particle emission during the pre-equilibrium process. All the calculations employ the same set of reaction ingredients, including the Koning–Delaroche optical model potential, the standard Lorentzian γ-ray strength function with RIPL-3 recommended parameters, and identical compound-nucleus decay schemes [55].

The only difference among the calculations arises from the NLD input. Three types of level densities are considered: the RHB-based combinatorial level densities obtained in the present study, HFB-based combinatorial level densities reported in Ref. [51], and those obtained using the phenomenological CTM.

To properly describe the experimental observables, mild renormalization of the level density at the neutron separation energy is applied in the standard form

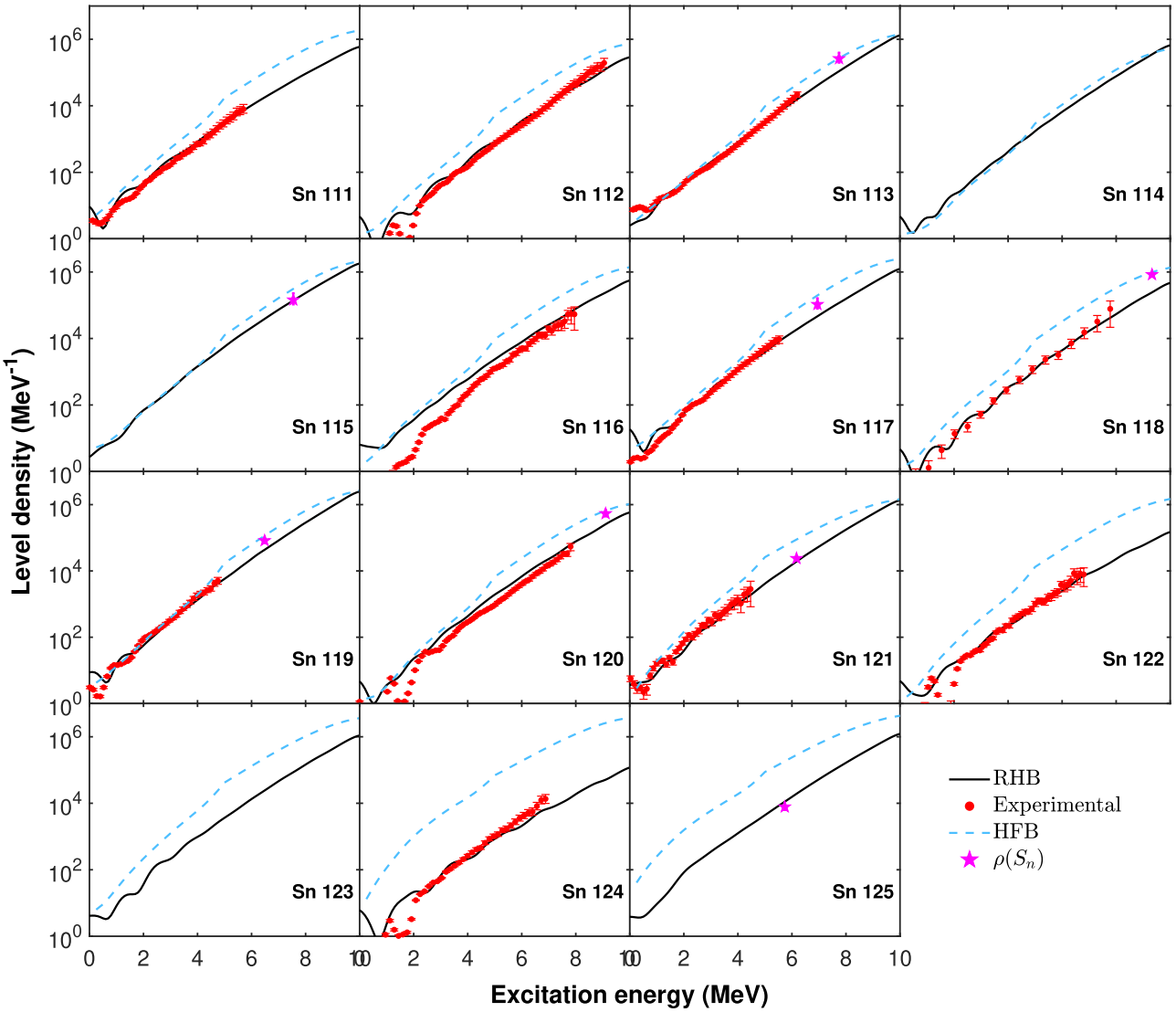

Fig. 3. (color online) Comparison of the NLDs of Sn isotopes calculated in the present study with experimental data extracted from the Oslo method and with results obtained using the nonrelativistic HFB plus combinatorial approach. The level density at the neutron separation energy, $\rho(S_n)$, deduced from s-wave neutron resonance spacings D_0 is also shown.

Table 2. Comparison of theoretical and experimental s-wave resonance spacings D_0.

Nucleus	N	$D_0^{\rm Theo}$/eV	$D_0^{\rm Expt}$/eV	$D_0^{\rm Theo}/D_0^{\rm Expt}$
^{113}Sn	63	376	157 ± 52	2.39
^{115}Sn	65	299	286 ± 106	1.04
^{117}Sn	67	865	380 ± 130	2.28
^{118}Sn	68	197	55 ± 5	3.59
^{119}Sn	69	908	480 ± 90	1.89
^{120}Sn	70	189	90 ± 20	2.10
^{121}Sn	71	2031	1640 ± 200	1.24
^{125}Sn	75	3488	5000 ± 1200	0.70

$$\rho_{\rm renorm}(U,J,P)=\exp\left[\alpha\sqrt{U-\delta}\right]\rho(U-\delta,J,P), \qquad (13)$$

with fixed parameters $\alpha=1$ and $\delta=0$ adopted consistently for all isotopes and level-density models. This standard choice corresponds to a mild, isotope-independent renormalization and enables a consistent comparison among different level-density models without requiring additional nucleus-by-nucleus adjustments.

The (n,γ) cross-sections for ^{116}Sn, ^{117}Sn, and ^{118}Sn, calculated using different NLD models, are compared with the experimental data obtained from the EXFOR library [40] (Fig. 4). All the calculations are performed within the same UNF framework, with differences arising solely from the level-density input.

For all the three isotopes, the (n,γ) cross-sections obtained using the RHB-based method are smaller than those obtained using the HFB-based approach over the entire neutron-energy range. At extremely low neutron

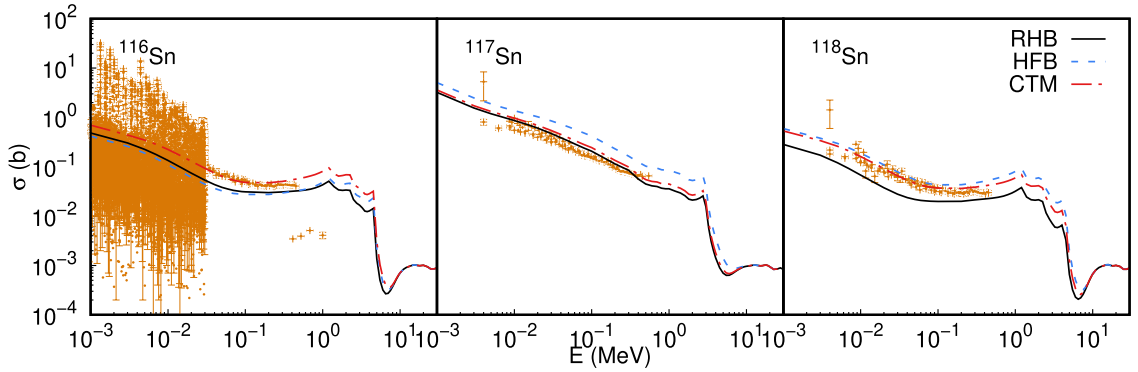

Fig. 4. (color online) Radiative neutron capture (n,γ) cross-sections for ^{116}Sn, ^{117}Sn, and ^{118}Sn, calculated using different NLD models, compared with experimental data obtained from the EXFOR library.

energies, the capture cross-section is influenced by the total level density as well as by the spin–parity distribution and channel competition; for ^{116}Sn, differences in spin-parity populations near the neutron separation energy may lead to slightly larger RHB-based cross-sections in the lowest-energy region.

This behavior reflects the differences in the underlying level densities, with the RHB-based combinatorial densities being systematically lower than the HFB-based ones. These results confirm that the choice of microscopic level density can lead to significant variations in predicted neutron capture cross-sections, with direct implications for nuclear reaction modeling and data evaluation.

IV. CONCLUSIONS AND OUTLOOK

Microscopic nuclear level densities of the Sn isotopic chain have been studied within a relativistic framework by combining the RHB theory with the combinatorial method. Self-consistent single-particle spectra and pairing correlations obtained from the covariant density functional theory provide the microscopic basis for the level-density construction in both even–even and odd-A nuclei.

The calculated level densities exhibit systematic trends with excitation energy and neutron number. At low excitation energies, pronounced odd–even effects and shell-related structures are observed, reflecting the underlying single-particle spectrum and pairing correlations. Comparisons with available experimental information, including cumulative low-lying levels, Oslo-type level densities, and s-wave neutron resonance spacings D_0, indicate that the present approach provides a consistent description of level densities along the Sn isotopic chain in the energy region where nuclear-structure effects are the most significant.

The impact of the microscopic level densities on nuclear reaction observables has been examined through radiative neutron capture (n,γ) cross-sections calculated within the statistical Hauser–Feshbach framework. Using identical reaction ingredients, systematic differences are observed between calculations based on relativistic and nonrelativistic microscopic level densities, reflecting the sensitivity of the statistical reaction observables to the NLD input.

This study demonstrates that microscopic NLDs constructed within a relativistic framework, especially by incorporating the finite-range separable pairing force, can be consistently applied in both nuclear-structure analyses and statistical reaction calculations. The RHB approach offers a more accurate description of pairing correlations, especially for mid-to-heavy nuclei such as the Sn isotopic chain and is thus an invaluable tool for nuclear reaction modeling. In future studies, this approach will be extended to a wider range of nuclei, including neutron-rich systems of astrophysical and technological interest. In addition, its systematic application in nuclear reaction modeling and nuclear data evaluation will be further explored, particularly for neutron-induced reactions.

ACKNOWLEDGMENTS

The authors thank Prof. Peter Ring (Technical University of Munich) for valuable discussions and insightful comments. They are also grateful to Yangping Shen (China Institute of Atomic Energy) for his support in the reliability analysis of the experimental data, to Pengxiang Du (Jilin University) for helpful guidance and constructive discussions, and to Xiaofei Jiang (Peking University) for useful advice.

References

[1] H. A. Bethe and R. F. Bacher, Rev. Mod. Phys. **8**, 82 (1936)
[2] H. A. Bethe, Rev. Mod. Phys. **9**, 69 (1937)
[3] P. Möller, A. Sierk, T. Ichikawa *et al.*, At. Data Nucl. Data Tables **109-110**, 1 (2016)

[4] C. Yalçın, Nuclear Science and Techniques **28**, 113 (2017)
[5] J. H. Luo, J. C. Liang, L. Jiang *et al.*, Nuclear Science and Techniques **34**, 4 (2023)
[6] P. H. Chen, H. Wu, Z. X. Yang *et al.*, Nuclear Science and Techniques **34**, 7 (2023)
[7] A. Gilbert and A. G. W. Cameron, Canadian Journal of Physics **43**, 1446 (1965)
[8] W. Dilg, W. Schantl, H. Vonach *et al.*, Nucl. Phys. A **217**, 269 (1973)
[9] A. Koning, S. Hilaire, and S. Goriely, Nucl. Phys. A **810**, 13 (2008)
[10] S. Hilaire, J. P. Delaroche, and M. Girod, Eur. Phys. J. A **12**, 169 (2001)
[11] F. C. Williams, Nucl. Phys. A **166**, 231 (1971)
[12] E. Beták and J. Dobeš, Zeitschrift für Physik A: Atoms and Nuclei **279**, 319 (1976)
[13] P. Obložinský, Nucl. Phys. A **453**, 127 (1986)
[14] S. Hilaire, J. Delaroche, and A. Koning, Nucl. Phys. A **632**, 417 (1998)
[15] Y. Alhassid, S. Liu, and H. Nakada, Physical Review Letters **83**, 4265 (1999)
[16] W. E. Ormand, Phys. Rev. C **56**, R1678 (1997)
[17] J. A. White, S. E. Koonin, and D. J. Dean, Phys. Rev. C **61**, 034303 (2000)
[18] N. Cerf, Phys. Rev. C **49**, 852 (1994)
[19] N. Cerf, Phys. Rev. C **50**, 836 (1994)
[20] B. Strohmaier, S. M. Grimes, and H. Satyanarayana, Phys. Rev. C **36**, 1604 (1987)
[21] S. M. Grimes and T. N. Massey, Phys. Rev. C **51**, 606 (1995)
[22] J. B. French and K. F. Ratcliff, Phys. Rev. C **3**, 94 (1971)
[23] N. D. Dang, N. Q. Hung, and L. T. Q. Huong, Phys. Rev. C **96**, 054321 (2017)
[24] N. Q. Hung, N. D. Dang, and L. T. Q. Huong, Phys. Rev. Lett. **118**, 022502 (2017)
[25] B. Dey, D. Pandit, S. Bhattacharya *et al.*, Phys. Rev. C **96**, 054326 (2017)
[26] B. Dey, N. Q. Hung, D. Pandit *et al.*, Phys. Lett. B **789**, 634 (2019)
[27] B. K. Agrawal and A. Ansari, Nucl. Phys. A **640**, 362 (1998)
[28] S. Goriely, Nucl. Phys. A **605**, 28 (1996)
[29] P. Decowski, W. Grochulski, A. Marcinkowski *et al.*, Nucl. Phys. A **110**, 129 (1968)
[30] P. Demetriou and S. Goriely, Nucl. Phys. A **695**, 95 (2001)
[31] T. Papenbrock and H. A. Weidenmüller, Rev. Mod. Phys. **79**, 997 (2007)
[32] S. Hilaire and S. Goriely, Nucl. Phys. A **779**, 63 (2006)
[33] S. Goriely, S. Hilaire, and A. J. Koning, Phys. Rev. C **78**, 064307 (2008)
[34] S. Hilaire, M. Girod, S. Goriely *et al.*, Phys. Rev. C **86**, 064317 (2012)
[35] S. Goriely, A.-C. Larsen, and D. Mücher, Phys. Rev. C **106**, 044315 (2022)
[36] S. Hilaire, S. Goriely, and S. Péru, , EPJ Web Conf. **322**, 06001 (2025)
[37] K.-P. Geng, P.-X. Du, J. Li *et al.*, Nuclear Science and Techniques **34**, 141 (2023)
[38] X. Jiang, X. Wu, P. Zhao *et al.*, Phys. Lett. B **849**, 138448 (2024)
[39] M. Markova, A. C. Larsen, P. von Neumann-Cosel *et al.*, Phys. Rev. C **109**, 054311 (2024)
[40] N. Otuka, E. Dupont, V. Semkova *et al.*, Nuclear Data Sheets **120**, 272 (2014)
[41] P. Ring, Prog. Part. Nucl. Phys. **37**, 193 (1996)
[42] D. Vretenar, A. Afanasjev, G. Lalazissis *et al.*, Physics Reports **409**, 101 (2005)
[43] G. A. Lalazissis, T. Niksic, D. Vretenar *et al.*, Phys. Rev. C **71**, 024312 (2005)
[44] Y. Tian, Z. Ma, and P. Ring, Phys. Lett. B **676**, 44 (2009)
[45] Y. Tian, Z.-Y. Ma, and P. Ring, Phys. Rev. C **79**, 064301 (2009)
[46] S. Goriely, S. Hilaire, and A. J. Koning, Astron. Astrophys. **487**, 767 (2008), arXiv: 0806.2239
[47] T. Døssing and A. Jensen, Nucl. Phys. A **222**, 493 (1974)
[48] W. Huang, M. Wang, F. Kondev *et al.*, Chin. Phys. C **45**, 030002 (2021)
[49] M. Wang, W. Huang, F. Kondev, G. Audi *et al.*, Chi. Phys. C **45**, 030003 (2021)
[50] J. Dobaczewski, P. Magierski, W. Nazarewicz *et al.*, Phys. Rev. C **63**, 024308 (2001)
[51] S. Goriely, M. Samyn, and J. M. Pearson, Phys. Rev. C **75**, 064312 (2007)
[52] J. Zhang, Nucl. Sci. Eng. **114**, 55 (1993)
[53] J. Zhang, Nucl. Sci. Eng. **116**, 35 (1994)
[54] J. Zhang, Nucl. Sci. Eng. **142**, 207 (2002)
[55] R. Capote, M. Herman, P. Obložinský, *et al.*, Nuclear Data Sheets **110**, 3107 (2009)